A common-reflection-point gather random noise attenuation method based on the synchrosqueezing wavelet transform

Xiaokai Wang[1], Zhizhou Huo[2], Dawei Liu[1], Weiwei Xu[1], and Wenchao Chen[1]

Abstract

Common-reflection-point (CRP) gather is one extensively used prestack seismic data type. However, CRP suffers more noise than a poststack seismic data set. The events in the CRP gather are always flat, and the effective signals from neighboring traces in the CRP gather have similar forms not only in the time domain, but also in the time-frequency (TF) domain. Therefore, we first use the synchrosqueezing wavelet transform (SSWT) to decompose seismic traces to the TF domain because the SSWT has better TF resolution and reconstruction properties. Then, we use the similarity of neighboring traces to smooth and threshold the SSWT coefficients in the TF domain. Finally, we used the modified SSWT coefficients to reconstruct the denoised traces for the CRP gather. Synthetic and field data examples indicate that our method can effectively attenuate random noise with a better attenuation performance than the commonly used principal component analysis, *f*-*x* filter, and the continuous wavelet transform method.

Introduction

Random noise follows an uncertain distribution and is one of the key factors in reducing the signal-to-noise ratio (S/N) of seismic records, which may further impact the precision of subsequent seismic inversion and interpretation severely. Therefore, random noise suppression plays a pivotal role in seismic data processing.

Random noise is considered independent with almost no temporal and spatial coherency. In contrast, effective signals are coherent in spatial direction and therefore predictable. Thus, prediction-based methods, including prediction filters (Gulunay, 1986; Chase, 1992) and projection filters (Chen and Sacchi, 2017), have been proposed to attenuate random noise. However, when the amplitude of random noise is relatively large, it is difficult to distinguish the noise from effective signals. To improve the denoising performance, random noise attenuation has been carried out in the transform domain with predefined transforms, such as the Fourier transform (Alsdorf, 1997), short-time Fourier transform (STFT) (Portnoff, 1980), Radon transform (Zhang et al., 2021), and curvelet transform (Neelamani et al., 2008). Useful signals always have relatively higher amplitude in the transform domain, whereas random noise is the opposite. Consequently, noise attenuation can be achieved by damping or thresholding the coefficients associated with random noise in the transform domain. However, based on the fact that useful signals are concentrated in the transform domain, whereas random noise is widespread, various studies have been taken to examine sparse representation in seismic data, aiming to represent the useful signals with as few atoms as possible with a given overcomplete dictionary (Elad et al., 2010). The construction of an overcomplete dictionary is the crucial step for successful denoising. In addition to the predefined dictionary, adaptive learning dictionary (Elad and Aharon, 2006; Beckouche and Ma, 2014) also has been one of the most well-known tools for assessing sparse representation for useful signals.

The low-rank property is a vital feature of the useful signals. Principal component analysis (PCA) (Hagen, 1982) and singular value decomposition (Jackson et al., 1991) are widely used in denoising for horizontal reflections. However, they introduce some artifacts when dealing with oblique or curve reflections. To enhance the capability of denoising for curve reflections, multichannel singular spectrum analysis (Oropeza and Sacchi, 2011) was proposed. Nuclear norm minimization (Kreimer et al., 2013) is another commonly used filtering method based on low-rank prior. Recently, considerable literature has grown up around the theme of deep learning. In addition, there has been extensive research on seismic data denoising using deep learning, such as 3D-denoising convolutional neural network (Liu et al., 2020b) and U-Net (Sun et al., 2020).

[1]Xi'an Jiaotong University, School of Information and Communication Engineering, Xi'an 710049, China. E-mail: xkwang@xjtu.edu.cn; liudawei2015@stu.xjtu.edu.cn; 544274644@qq.com; wencchen@xjtu.edu.cn (corresponding author).
[2]SINOPEC Petroleum Exploration and Production Research Institute, Beijing 100083, China. E-mail: kboby246@163.com.
Manuscript received by the Editor 9 February 2021; revised manuscript received 12 October 2021; published online 20 January 2022. This paper appears in *Interpretation*, Vol. 10, No. 1 (February 2022); p. SA59–SA67, 9 FIGS., 3 TABLES.
http://dx.doi.org/10.1190/INT-2021-0049.1.

There are many kinds of seismic data such as VSP data, prestack gather, and poststack data set with different characteristics. Exploring and making full use of the data characteristics can improve the results of noise attenuation. The common-reflection-point (CRP) gather contains much more information than the stacked data set; thus, it is frequently used in amplitude-variation-with-offset analysis. CRP gathers basically eliminate the influence of interface bending and inclined strata; therefore, they have relatively horizontal reflections. Based on this, Xu et al. (2015) designed a workflow with a structure median filter to attenuate random noise in CRP gather. Liu et al. (2020a) used a multiscale network to extract the self-similar features in CRP gather and obtained a good noise attenuation result. Based on the assumption that neighboring traces have similar waveforms and almost the same time delay, Zhou et al. (2019) thought CRP had a low-rank prior and applied PCA to attenuate random noise in CRP gather. However, it is very difficult to choose the rank. The Fourier transform can be used to suppress the random noise by choosing the frequency band of the signal. However, it cannot fully use the spatial correlation between neighboring traces in the CRP gather. The similar neighboring traces also generate similar time-frequency (TF) spectra. Therefore, decomposing each trace in CRP gather to the TF domain is beneficial for using TF similarity to further attenuate the random noise. STFT, the Stockwell transform (ST), and continuous wavelet transform (CWT) are some frequently used TF transforms. Compared with the fixed window length in STFT, CWT can adjust its window length at different frequencies. Meanwhile, CWT can adjust its mother wavelet to match real seismic data. Therefore, CWT is extensively used in seismic data processing and interpretation. However, CWT is limited by the Gabor-Heisenberg uncertainty principle. Therefore, it suffers from the limited TF resolution. TF spectrum reassignment (SRM) (Plante et al., 1998) can improve TF resolution by moving CWT coefficients to its gravity center. The synchrosqueezing wavelet transform (SSWT) (Daubechies et al., 2011) moves the CWT coefficients only along the frequency axis. These two methods (SRM and SSWT) can make the TF spectrum more concentrated. Thus, they are frequently used

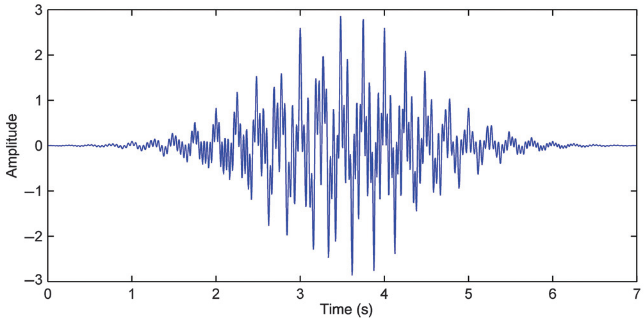

Figure 1. A complex signal with three components ($x_1(t)= e^{-2*(t-3.5)^2}e^{j26\pi t}$, $x_2(t) = e^{-2*(t-3.5)^2}e^{j2\pi(16\ t+t^2)}$, and $x_3(t) = e^{-0.25(t-3.5)^2}[1.5+\cos(\pi t)]e^{j2\pi(25\ t+\sin(\pi t))}$).

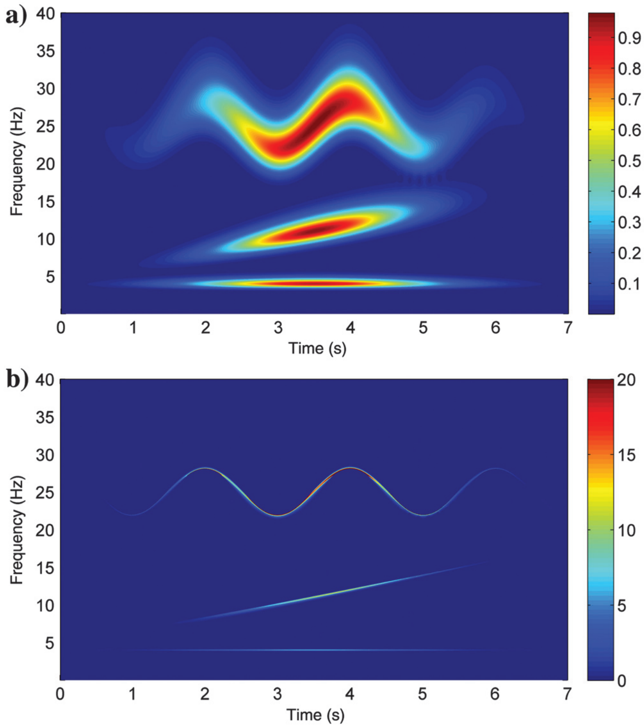

Figure 2. TF spectra of the signal shown in Figure 1 by using (a) CWT and (b) SSWT. SSWT has shown its much higher TF resolution than the CWT for these components.

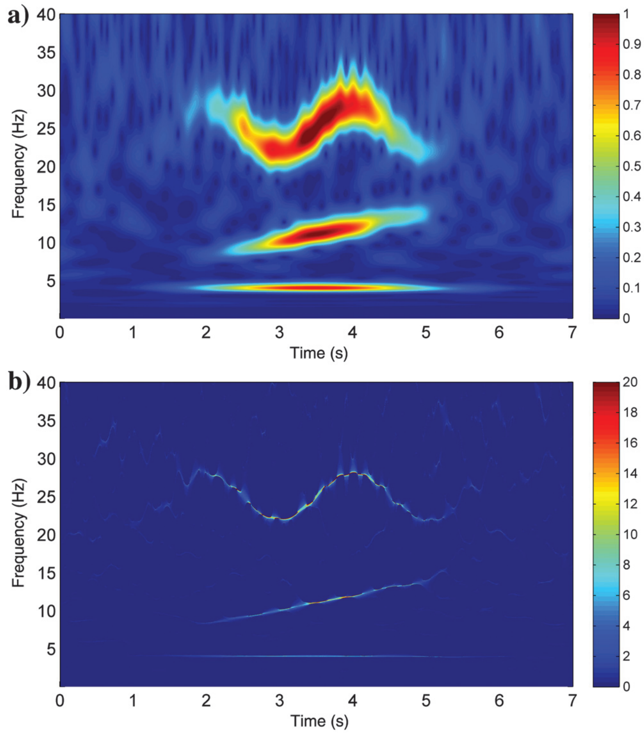

Figure 3. TF spectra of the signal shown in Figure 1 after adding Gaussian white noise by using (a) CWT and (b) SSWT. SSWT can give a high-TF resolution and better antinomies' performance.

in spectrum decomposition and other seismic applications (Wang et al., 2014, 2019, 2020; Tao et al., 2019). Compared with SRM, SSWT can decompose the signal to the TF domain and has a better TF resolution than CWT. Furthermore, SSWT has the reconstruction ability and certain antinoise ability. Therefore, SSWT has been used in random noise suppression for single traces. In this work, we use SSWT to decompose each trace in CRP gathers and further use neighboring TF similarity to modify SSWT coefficients to attenuate random noise in the CRP gather.

This paper is organized as follows. First, we will present SSWT and introduce the proposed random noise attenuation in CRP gathers based on SSWT. Second, the proposed method is applied to one synthetic data set and one field data set to demonstrate its effectiveness. Finally, we draw the conclusions.

Methods

CWT

For an arbitrary 1D signal $x(t)$, its Fourier transform $X(\omega)$ is defined by

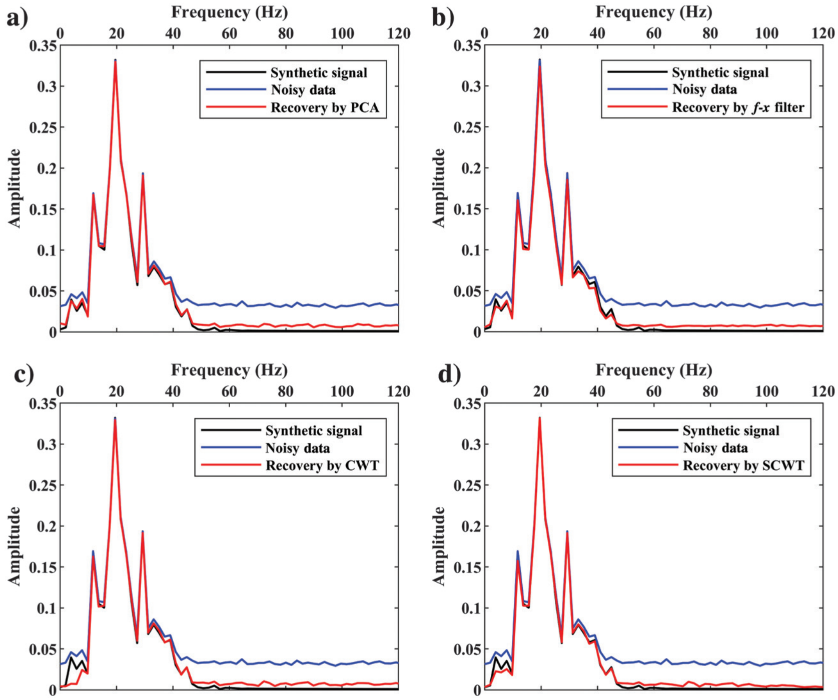

Figure 5. Amplitude spectrum. (a) Amplitude spectrum of the synthetic signal, the noisy data, and the recovered results by the PCA. (b) Amplitude spectrum of the synthetic signal, the noisy data, and the recovered results by the f-x filter. (c) Amplitude spectrum of the synthetic signal, the noisy data, and the recovered results by the CWT. (d) Amplitude spectrum of the synthetic signal, the noisy data, and the recovered results by the SCWT.

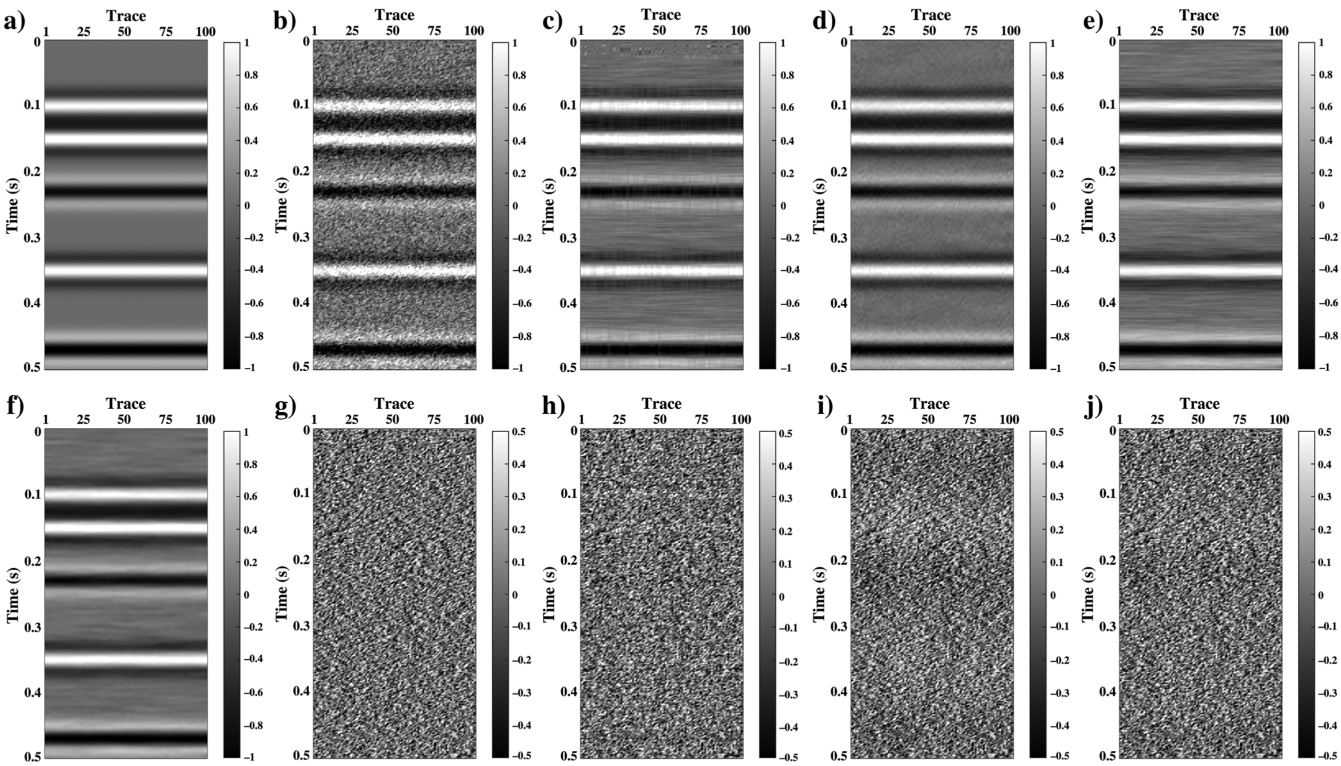

Figure 4. Results of one synthetic data set. (a) Synthetic signal. (b) Noisy data set. (c) Recovered result using PCA. (d) Recovered result using f-x filter. (e) Recovered result using CWT. (f) Recovered result using SCWT. (g) The suppressed noise section using PCA. (h) The suppressed noise section using the f-x filter. (i) The suppressed noise section using CWT. (j) The suppressed noise section using SCWT.

$$X(\omega) = \int_{-\infty}^{+\infty} x(t) e^{-j\omega t} dt, \quad (1)$$

where t and ω are the time and frequency variables, respectively. The j in equation 1 represents the imaginary unit. If a mother wavelet $\psi(t)$ satisfies the admissibility condition:

$$0 < \int_{0}^{+\infty} \frac{|\Psi(\omega)|^2}{\omega} d\omega < +\infty, \quad (2)$$

where $\Psi(\omega)$ is the Fourier transform of $\psi(t)$; then, the CWT of $x(t)$ is defined as the inner-product of signal $x(t)$ and the scaled and shifted wavelets (Mallat, 1998):

Table 1. PS/Ns of different noise attenuating methods' result for noisy data sets with different noise levels. The large value means the S/N is high. Therefore, we use bold values to highlight the method has the largest S/N.

Noisy data set	CWT method	PCA	f-x filter	Proposed method
18.09	30.76	29.76	33.05	**35.05**
12.07	24.47	23.65	27.21	**28.91**
6.05	19.07	17.29	21.11	**23.08**
0.03	13.30	10.21	15.10	**17.24**

Table 2. The crosscorrelation between the synthetic signal and four noise suppression results. The large value means the similarity between the denoised result and clean signal is high. Therefore, we use bold values to highlight the method has the highest similarity between the denoised result and clean signal.

Noisy data's PS/N	Xcorr (signal, CWT)	Xcorr (signal, PCA)	Xcorr (signal, f-x)	Xcorr (signal, SCWT)
18.09	0.9966	0.9958	0.9982	**0.9987**
12.07	0.9857	0.9831	0.9926	**0.9948**
6.05	0.9520	0.9321	0.9685	**0.9801**
0.03	0.8418	0.7350	0.8717	**0.9215**

Table 3. The crosscorrelation between the added noise and the suppressed noise. The large value means the similarity between the suppressed noise and the added noise is high. Therefore, we use bold values to highlight the method has the highest similarity between the suppressed noise and the added noise.

Noisy data's PS/N	Xcorr (noise, CWT_diff)	Xcorr (noise, PCA_diff)	Xcorr (noise, f-x_diff)	Xcorr (noise, SCWT_diff)
18.09	0.9726	0.9654	0.9839	**0.9899**
12.07	0.9708	0.9646	0.9846	**0.9896**
6.05	0.9748	0.9617	0.9843	**0.9901**
0.03	0.9762	0.9509	0.9844	**0.9905**

$$\mathrm{CWT}_x^{\psi(t)}(t,a) = \frac{1}{a}\int_{-\infty}^{+\infty} x(\tau)\psi^*\left(\frac{\tau - t}{a}\right) d\tau, \quad (3)$$

where $z*$ represents the complex conjugate of z. In addition, a and t are scale and time variables of CWT, respectively. Furthermore, the CWT of $x(t)$ also can be computed in the frequency domain:

$$\mathrm{CWT}_x^{\psi(t)}(t,a) = \int_{-\infty}^{+\infty} X(\omega)\Psi^*(a\omega) e^{j\omega t} d\omega. \quad (4)$$

If we further suppose that $\psi(t)$ is an analytic wavelet, which means that the support region of $\Psi(\omega)$ only locates in the positive frequency axis and the supremum of $|\Psi(\omega)|$ equals to one, then a real-valued signal can be reconstructed by summing up all CWT coefficients along the scale axis (Gao et al., 1999):

$$x(t) = 2\mathrm{REAL}\left\{\frac{1}{C_\psi}\int_{0}^{+\infty} \mathrm{CWT}_x^{\psi(t)}(t,a)\frac{da}{a}\right\}, \quad (5)$$

where $C_\psi = \int_0^{+\infty}(|\Psi(\omega)|/\omega)d\omega$ and REAL$\{z\}$ represents the real part of the complex number z.

SSWT

Although CWT can adjust its window width for different scales, its TF resolution is still restricted by the uncertainty principle like other linear TF transforms, such as STFT, and ST. To improve the TF resolution, one classical method is the TF SRM (Plante et al., 1998), which moves the TF energy to the gravity center. For CWT, its gravity center can be defined by the group delay $\hat{t}(t,a)$ and instantaneous frequency (IF) $\hat{\omega}(t,a)$ (Auger and Flandrin, 1995):

$$\hat{t}(t,a) = \frac{1}{a}\frac{\int_{-\infty}^{+\infty}\tau x(\tau)\psi^*(\frac{\tau-t}{a})d\tau}{\mathrm{CWT}_x^{\psi(t)}(t,a)}, \quad (6)$$

$$\hat{\omega}(t,a) = (-j)\frac{\partial_t \mathrm{CWT}_x^{\psi(t)}(t,a)}{\mathrm{CWT}_x^{\psi(t)}(t,a)}. \quad (7)$$

Then, the SRM of CWT can be easily obtained by

$$\begin{aligned}\mathrm{SRM\_CWT}(t,\omega) &= \int_{R^2}\mathrm{CWT}_x^{\psi(t)}(t,a)\delta[t-\hat{t}(t,a)] \\ &\times \delta[\omega - \hat{\omega}(t,a)]d\tau\frac{da}{a}. \quad (8)\end{aligned}$$

where $\delta(\cdot)$ represents the Dirac delta function. Although the SRM can improve CWT's TF resolution, it cannot be used to reconstruct the signal because the SRM moves CWT coefficients along frequency direction and time direction. To balance the TF resolution and reconstruction property, SSWT discards moving CWT coefficients along the time direction and only moves coefficients along the frequency direction:

$$\mathrm{SSWT}(t,\omega)=\int_{R}\mathrm{CWT}_{x}^{\psi(t)}(t,a)\delta[\omega-\hat{\omega}(t,a)]\frac{da}{a}. \quad (9)$$

Then, the signal can be reconstructed by SSWT like equation 5:

$$x(t)=2\mathrm{REAL}\{\int_{0}^{+\infty}\mathrm{SSWT}(t,\omega)d\omega\}. \quad (10)$$

In addition, the signal also can be reconstructed by restricting an integration range to reconstruct the component in the complicated signal.

A complex signal with three components ($x_1(t)=e^{-2*(\mathrm{t}-3.5)^2}e^{j26\pi t}$, $x_2(t)=e^{-2*(\mathrm{t}-3.5)^2}e^{j2\pi(16\ t+t^2)}$, and $x_3(t)=e^{-0.25(\mathrm{t}-3.5)^2}[1.5+\cos(\pi t)]e^{j2\pi(25\ t+\sin(\pi t))}$) is shown in Figure 1. The Morlet with a modulating frequency of 10 rad/s is chosen as the mother wavelet. Then, CWT and SSWT are applied to this complex signal. The corresponding TF spectra of these two TF methods are shown in Figure 2a and 2b, with a frequency interval of 0.1 Hz. SSWT has shown its much higher TF resolution than the CWT for these components. To further test the SSWT's performance, Gaussian white noise is added to the synthetic signal in Figure 1. The results of CWT and SSWT on the noisy signal are shown in Figure 3a and 3b, respectively. SSWT can give a higher TF resolution and better antinoise performance than CWT.

CRP gather random noise attenuation based on SSWT

CRP is one of the frequently used prestack seismic data sets. However, CRP suffers more random noise than the poststack seismic data set. In the CRP gather, effective signals from neighboring traces have similar waveforms, whereas the random noise in neighboring traces is independent from each other. Furthermore, the lateral changes between the neighboring seismic traces in the CRP are not severe. Therefore, in the TF domain, the distributions of effective signals are similar, whereas the distributions of the random noise are different. Because SSWT has a better TF concentration and better antinoise performance, we use the SSWT to decompose each trace in the CRP gather and further use the neighboring similarity in TF domain to attenuate random noise for the CRP gather.

Suppose that the mth trace in the CRP gather is $x_m(t)$, we use $\mathrm{SSWT}(x_m;t,\omega)$ to represent the SSWT of $x_m(t)$. We can generate a mask function $\mathrm{Mask}_{\mathrm{SSWT}}(x_m;t,\omega)$ for $\mathrm{SSWT}(x_m;t,\omega)$ by using the threshold $e1$:

$$\mathrm{Mask\_SSWT}(x_m;t,\omega)=\begin{cases}1, & |\mathrm{SSWT}(x_m;t,\omega)|\geq e1\\ 0, & |\mathrm{SSWT}(x_m;t,\omega)|<e1\end{cases}. \quad (11)$$

Usually, the CWT coefficients related to useful signals have strong correlation in the time-scale plane; thus, they can accumulate to the IF position in equation 7. The $e1$ can be obtained by the random noise's variance. However, the CWT coefficients related to random noise

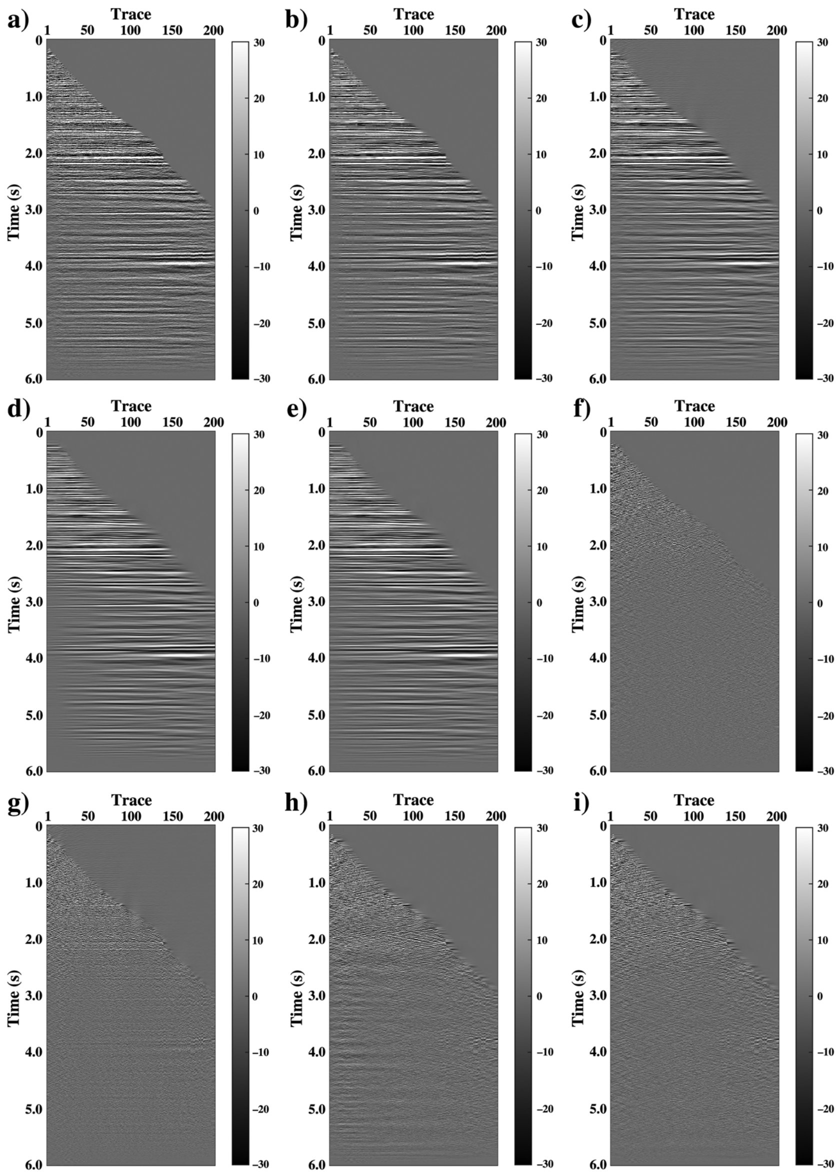

Figure 6. Results of field prestack data. (a) Noisy data. (b) Recovered result using PCA. (c) Recovered result using f-x filter. (d) Recovered result using CWT. (e) Recovered result using SCWT. (f) The suppressed noise section using PCA. (g) The suppressed noise section using the f-x filter. (h) The suppressed noise section using CWT. (i) The suppressed noise section using SCWT.

cannot accumulate in the synchrosqueezing procedure. Therefore, the signal-related SCWT coefficients have relatively higher values, whereas the noise-related SCWT coefficients have lower values (as shown in Figure 3b). We consider a spatial window including $2p+1$ traces. When we focus on noise attenuation for the mth trace, the weighted average SSWT Mean_SSWT $(x_m;t,\omega)$ can be obtained by

$$\begin{aligned}&\mathrm{Mean\_SSWT}(x_m;t,\omega)\\&\quad=\sum_{n=-p}^{p}\frac{|\mathrm{SSWT}(x_{m+n};t,\omega)|}{\mathrm{QSSWT}(x_m;t,\omega)}\mathrm{SSWT}(x_{m+n};t,\omega)\end{aligned} \tag{12}$$

where

$$\mathrm{QSSWT}(x_m;t,\omega)=\sum_{n=-p}^{p}|\mathrm{SSWT}(x_{m+n};t,\omega)|. \tag{13}$$

Furthermore, we can generate the final mask function FMask_SSWT$(x_m;t,\omega)$ for the mth trace in the CRP gather by all mask functions within the spatial window:

$$\begin{aligned}&\mathrm{FMask\_SSWT}(x_m;t,\omega)\\&\quad=1-\prod_{n=-p}^{p}(1-\mathrm{Mask\_SSWT}(x_{m+n};t,\omega)).\end{aligned} \tag{14}$$

Finally, the noise attenuation result $\hat{x}_m(t)$ for the mth trace can be obtained by the weighted average SSWT Mean_SSWT$(x_m;t,\omega)$ and the final mask function FMask_SSWT$(x_m;t,\omega)$:

$$\begin{aligned}\hat{x}_m(t)=2\mathrm{REAL}[&\int_0^{+\infty}\mathrm{Mean\_SSWT}(x_m;t,\omega)\\&\times\mathrm{FMask\_SSWT}(x_m;t,\omega)d\omega].\end{aligned} \tag{15}$$

Results

Synthetic data example

The proposed method is applied to a synthetic prestack seismic data set, which contains 100 traces. Each trace has 251 sampling points with a 2 ms interval. Figure 4a shows the synthetic signal. Some random noise is added to this signal, and the corresponding noisy data set is shown in Figure 4b. Because the reflected events are approximately horizontal, leading to the low-rank characteristic, we apply the PCA method to this data set for comparison. Moreover, the well-known f-x filter method also is chosen as one comparison method. Furthermore, because CWT can replace the SSWT in the proposed method, then a CWT-based denoising method (CWT method) can be obtained. The PCA method, f-x filter, CWT method, and the proposed method share the same spatial window size. These four methods are applied to the noisy data set in Figure 4b, and their noise suppression results are shown in Figure 4c–4f, respectively. These four methods can suppress most of the random noise. However, compared with the other three methods' results, the proposed method does not have the clear noise residue in the signal section (Figure 4f).

We also compute the differences between the noisy data set (Figure 4b) and the four results (Figure 4c–4f) and show these suppressed noises in Figure 4g–4j, respectively. Compared with the other three methods' suppressed noise, our SSWT-based method does not have the visible signal structure in the noise section (Figure 4j). Furthermore, the corresponding average amplitude spectra of the synthetic signal, the noisy data, and the recovered results by the four methods are plotted in Figure 5a–5d. We can see that the average amplitude spectrum of the recovered result by our method is almost identical to the average amplitude spectrum of the synthetic signal, which proves the superiority of our proposed method.

To quantitatively evaluate the four methods' performance, different levels of random noise are added to the clean signal to generate some noisy data sets with a different S/N. The four methods are applied to these noisy data sets. The peak signal-to-noise ratio (PS/N) is used to measure the performance of the different methods quantitatively. The PS/Ns of four methods at different

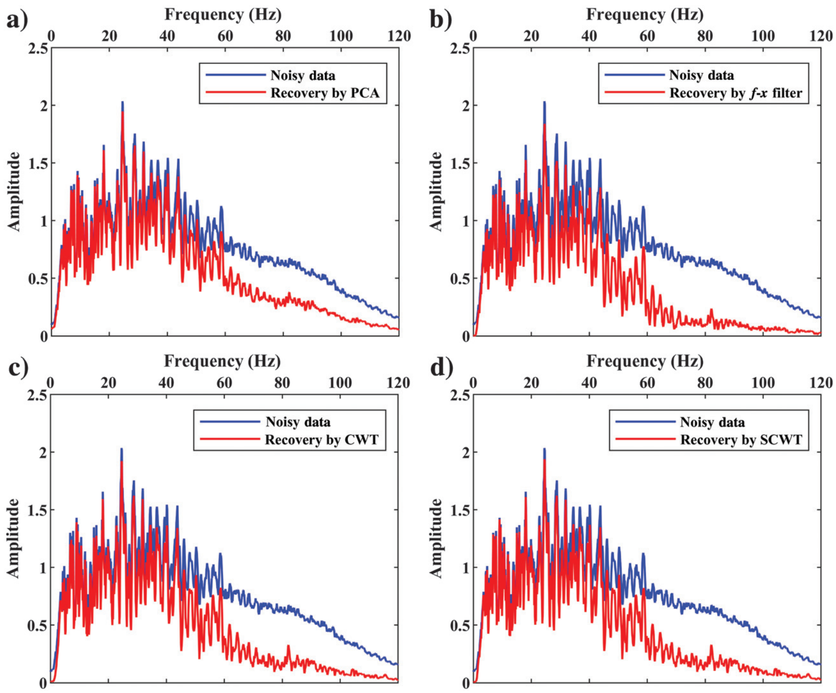

Figure 7. Amplitude spectrum. (a) Amplitude spectrum of the noisy data, and the recovered results by the PCA. (b) Amplitude spectrum of the noisy data, and the recovered results by the f-x filter. (c) Amplitude spectrum of the noisy data, and the recovered results by the CWT. (d) Amplitude spectrum of the noisy data, and the recovered results by the SCWT.

noise levels are shown in Table 1. Compared with the other three methods, our method enhances the PS/N by more than 2 dB for the different noisy data set.

Furthermore, the crosscorrelations between the pure synthetic signal and different noise suppression results are computed and shown in Table 2. Our results (the fifth column) have the highest crosscorrelations than the other three methods' results. Meanwhile, the crosscorrelations
between the added and suppressed noise also are computed and shown in Table 3. It is evident that our method also provides higher crosscorrelations than other methods.

Therefore, we can conclude that our method has a stronger random noise suppression ability than the other three methods.

For better comparison, we magnify the target areas during periods of 2.0–4.0 s. Figure 8a shows that the deep-layer data set of 2.0–4.0 s is seriously affected by strong random noise. For the PCA method, we can see that there still exist lots of residual noise in Figure 8b, especially in the area indicated by the white arrow. The f-x filter method damages some flat events, especially in the parts indicated by the yellow arrow in Figure 8g. The CWT method has some useful signal leakages highlighted by the black rectangle in Figure 8h. However,

Real data example

We apply our method to a field prestack seismic data set containing 300 CRP gathers with 200 traces for each gather. Each trace has 3001 sampling points with a 2 ms interval. Figure 6a shows one CRP extracted from the field data set, and it can be seen that there is a large amount of random noise, which highly masks the useful signals. Same as the synthetic data example, PCA, f-x filter, and CWT method are used for comparison. Figure 6b–6e shows the noise attenuation results by three comparison methods and the proposed method, respectively. We can observe that there is still a large portion of random noise in Figure 6b and 6c, which breaks the continuity of the useful events. In contrast, as shown in Figure 6d and 6e, the results of the CWT method and the proposed method can exhibit some clear events. Figure 6f–6i shows the suppressed noise sections of the four methods. The noise attenuated by the PCA method (Figure 6f) is much less than the noise attenuated by the other three methods. In the noise section of the f-x filter (Figure 6g), there are some signal residuals. In addition, we find some useful low-frequency signal leakages for the CWT method (Figure 6h). The proposed method (Figure 6i) can suppress as much noise as possible while maintaining a valid signal. To prove the effectiveness of the presented method quantitatively, we show the corresponding average amplitude spectrum of the original noisy data and the recovered results by different methods in Figure 7. It is concluded that our proposed method removes more high-frequency components, which reconciles with the fact that the random noise has mainly high-frequency energy.

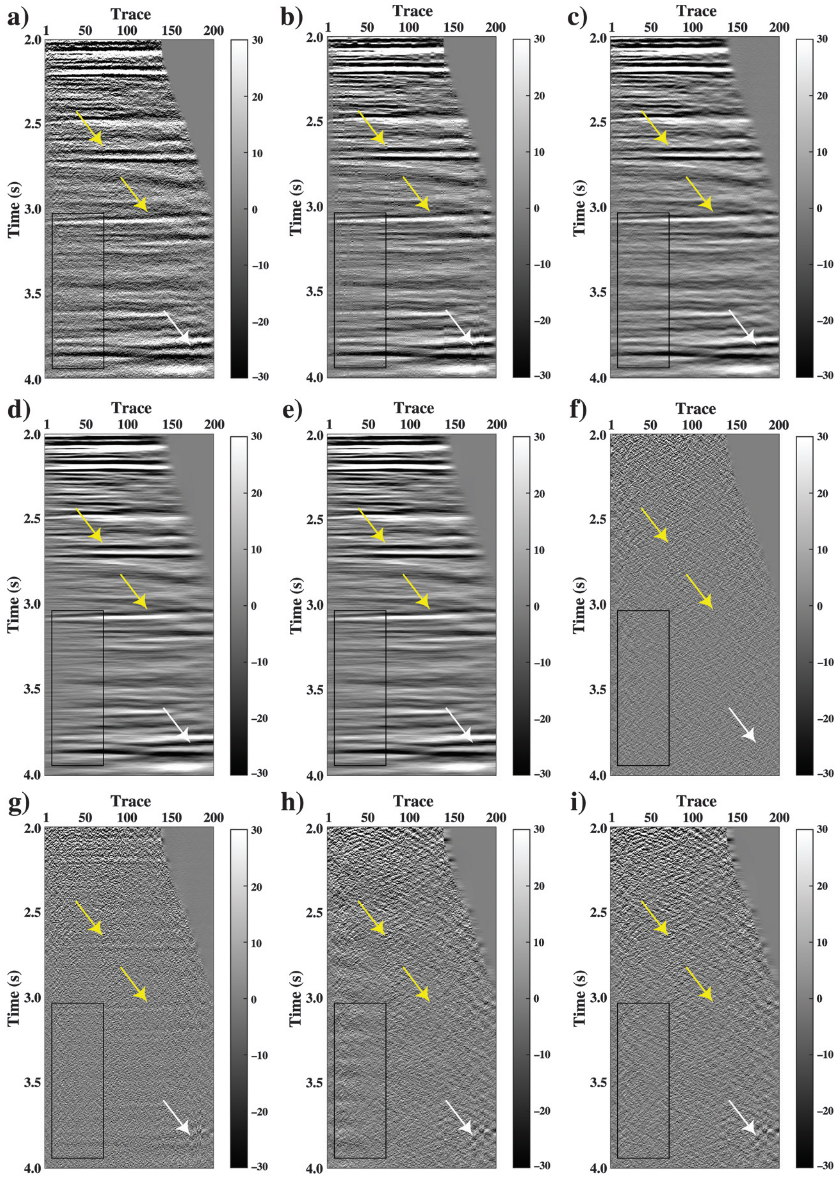

Figure 8. Results of target areas during periods of 2.0–4.0 s. (a) Noisy data. (b) Recovered result using PCA. (c) Recovered result using f-x filter. (d) Recovered result using CWT. (e) Recovered result using SCWT. (f) The suppressed noise section using PCA. (g) The suppressed noise section using the f-x filter. (h) The suppressed noise section using CWT. (i) The suppressed noise section using SCWT.

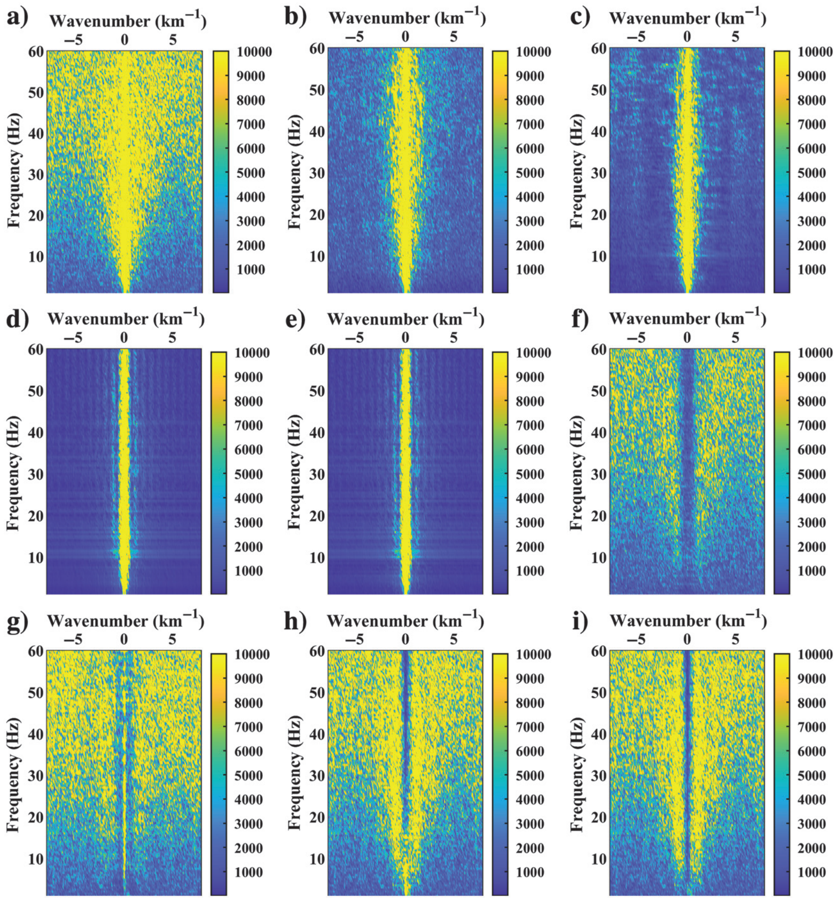

Figure 9. Corresponding f-k spectrum of results of target areas during periods of 2.0–4.0 s. (a) Noisy data. (b) Recovered result using PCA. (c) Recovered result using f-x filter. (d) Recovered result using CWT. (e) Recovered result using SCWT. (f) The suppressed noise section using PCA. (g) The suppressed noise section using the f-x filter. (h) The suppressed noise section using CWT. (i) The suppressed noise section using SCWT.

the proposed method (Figure 8e) has less random noise than the results of other methods. There is no apparent useful signal in the corresponding noise section of Figure 8i. Furthermore, the f-k spectra of Figure 8a–8i are shown in Figure 9a–9i, respectively. We can see that, although most useful signal frequency components are retained by the PCA method, there are still lots of random noise residuals, as shown in Figure 9b and 9f. Compared with the PCA method, the f-x filter method (Figure 9c and 9g) and the CWT method (Figure 9d and 9h) remove more random noise frequency components, but they damage some useful signal frequency components. Our method suppressed random noise thoroughly (Figure 9e) and well preserved the useful signal (Figure 9i).

Conclusions

In this paper, a CRP gather random noise attenuation method based on synchrosqueezing transform is proposed. SSWT is used to decompose each trace in CRP gather to the TF domain. The spatial smoothed TF result is filtered by a TF mask function, which is generated by the neighboring TF results. The synthetic and field data examples have shown that the proposed method can attenuate more random noise and well preserve useful signals than the classical PCA method, f-x filter method, and CWT method. The proposed method is designed for CRP gather because the events in CRP gather are flat. Therefore, the proposed method cannot be used for other kinds of prestack gathers and poststack data sets. In the future research, the proposed method could be used for other kinds of seismic data set by flattening the events first.

Acknowledgments

The work is supported by the National Natural Science Foundation of China (41974131 and 41774135). We would like to thank the Exploration and Development Research Institute of Daqing Oilfield Company Ltd. for providing the data set.

Data and materials availability

Data associated with this research are confidential and cannot be released.

References

Alsdorf, D., 1997, Noise reduction in seismic data using Fourier correction coefficient filtering: Geophysics, **62**, 1617–1627, doi: 10.1190/1.1444264.

Auger, F., and P. Flandrin, 1995, Improving the readability of time-frequency and time-scale representations by the reassignment method: IEEE Transactions on Signal Processing, **43**, 1068–1089, doi: 10.1109/78.382394.

Beckouche, S., and J. Ma, 2014, Simultaneous dictionary learning and denoising for seismic data: Geophysics, **79**, no. 3, A27–A31, doi: 10.1190/geo2013-0382.1.

Chase, M. K., 1992, Random noise reduction by 3-D spatial prediction filtering: 62nd Annual International Meeting, SEG, Expanded Abstracts, 1152–1153, doi: 10.1190/1.1821933.

Chen, K., and M. D. Sacchi, 2017, Robust f-x projection filtering for simultaneous random and erratic seismic noise attenuation: Geophysical Prospecting, **65**, 650–668, doi: 10.1111/1365-2478.12429.

Daubechies, I., J. Lu, and H.-T. Wu, 2011, Synchrosqueezed wavelet transforms: An empirical mode decomposition-like tool: Applied and Computational Harmonic Analysis, **30**, 243–261, doi: 10.1016/j.acha.2010.08.002.

Elad, M., and M. Aharon, 2006, Image denoising via sparse and redundant representations over learned dictionaries: IEEE Transactions on Image Processing, **15**, 3736–3745, doi: 10.1109/TIP.2006.881969.

Elad, M., M. A. T. Figueiredo, and Y. Ma, 2010, On the role of sparse and redundant representations in image processing: Proceedings of the IEEE, **98**, 972–982, doi: 10.1109/JPROC.2009.2037655.

Gao, J., X. Dong, W. B. Wang, Y. Li, and C. Pan, 1999, Instantaneous parameters extraction via wavelet transform: IEEE Transactions on Geoscience and Remote Sensing, **37**, 867–870, doi: 10.1109/36.752206.

Gulunay, N., 1986, FXDECON and complex Wiener prediction filter: 56th Annual International Meeting, SEG, Expanded Abstracts, 279–281, doi: 10.1190/1.1893128.

Hagen, D. C., 1982, The applications of principle components analysis to seismic data sets: Geoexploration, **20**, 93–111, doi: 10.1016/0016-7142(82)90009-6.

Jackson, G. M., I. M. Mason, and S. A. Greenhalgh, 1991, Principal component transforms of triaxial recordings by singular value decomposition: Geophysics, **56**, 528–533, doi: 10.1190/1.1443068.

Kreimer, N., A. Stanton, and M. Sacchi, 2013, Tensor completion based on nuclear norm minimization for 5D seismic data reconstruction: Geophysics, **78**, no. 6, V273–V284, doi: 10.1190/geo2013-0022.1.

Liu, D., Z. Deng, C. Wang, X. Wang, and W. Chen, 2020a, An unsupervised deep learning method for denoising prestack random noise: IEEE Geoscience and Remote Sensing Letters, 1–5, doi: 10.1109/LGRS.2020.3019400.

Liu, D., W. Wang, X. Wang, C. Wang, J. Pei, and W. Chen, 2020b, Poststack seismic data denoising based on 3-D convolutional neural network: IEEE Transactions on Geoscience and Remote Sensing, **58**, 1598–1629, doi: 10.1109/TGRS.2019.2947149.

Mallat, S., 1998, A wavelet tour of signal processing: Academic Press.

Neelamani, R., A. I. Baumstein, D. G. Gillard, M. T. Hadidi, and W. L. Soroka, 2008, Coherent and random noise attenuation using the curvelet transform: The Leading Edge, **27**, 240–248, doi: 10.1190/1.2840373.

Oropeza, V., and M. Sacchi, 2011, Simultaneous seismic data denoising and reconstruction via multichannel singular spectrum analysis: Geophysics, **76**, no. 3, V25–V32, doi: 10.1190/1.3552706.

Plante, F., G. Meyer, and W. A. Ainsworth, 1998, Improvement of speech spectrogram accuracy by the method of reassignment: IEEE Transactions on Speech and Audio Processing, **6**, 282–287, doi: 10.1109/89.668821.

Portnoff, M., 1980, Time-frequency representation of digital signals and systems based on short-time Fourier analysis: IEEE Transactions on Acoustics, Speech, and Signal Processing, **28**, 55–69, doi: 10.1109/TASSP.1980.1163359.

Sun, J., S. Slang, T. Elboth, T. L. Greiner, S. McDonald, and L.-J. Gelius, 2020, Attenuation of marine seismic interference noise employing a customized U-Net: Geophysical Prospecting, **68**, 845–871, doi: 10.1111/1365-2478.12893.

Tao, Y., S. Cao, Y. Ma, and M. Ma, 2019, Second-order adaptive synchrosqueezing *S* transform and its application in seismic ground roll attenuation: IEEE Geoscience and Remote Sensing Letters, **17**, 1308–1312, doi: 10.1109/LGRS.2019.2946368.

Wang, P., J. Gao, and Z. Wang, 2014, Time-frequency analysis of seismic data using synchrosqueezing transform: IEEE Geoscience and Remote Sensing Letters, **11**, 2042–2044, doi: 10.1109/LGRS.2014.2317578.

Wang, X., W. Chen, J. Wen, J. Ning, and J. Li, 2019, The applications of synchrosqueezing time-frequency analysis in high-speed train induced seismic data processing: Chinese Journal of Geophysics, **62**, 2328–2335.

Wang, X., B. Wang, and W. Chen, 2020, The second-order synchrosqueezing continuous wavelet transform and its application in the high-speed-train induced seismic signal: IEEE Geoscience and Remote Sensing Letters, **18**, 1109–1113, doi: 10.1109/LGRS.2020.2993596.

Xu, L., Z. Liu, X. Wang, J. Xie, and C. Jia, 2015, Optimization technology based on structure median filter for CRP gathers: Progress in Geophysics, **30**, 1804–1810.

Zhang, Q., H. Wang, W. Chen, and G. Huang, 2021, A robust method for random noise suppression based on the Radon transform: Journal of Applied Geophysics, **184**, 104183, doi: 10.1016/j.jappgeo.2020.104183.

Zhou, J., G. Ma, B. Sui, W. Xu, W. Zhang, Y. Zeng, and H. Lu, 2019, Application research of PCA algorithm in optimization process of CRP gathers: Progress in Geophysics, **34**, 1577–1583.

Biographies and photographs of the authors are not available.